JOURNAL OF SPACECRAFT AND ROCKETS
Vol. 52, No. 5, September–October 2015

Safe Picosatellite Release from a Small Satellite Carrier

Martin Wermuth* and Gabriella Gaias*
DLR, German Aerospace Center, 82234 Oberpfaffenhofen, Germany
and
Simone D'Amico†
Stanford University, Stanford, California 94305

DOI: 10.2514/1.A33036

The Berlin Infrared Optical System satellite, which is scheduled for launch in 2016, will carry onboard a picosatellite and release it through a spring mechanism. After separation, it will perform proximity maneuvers in formation with the picosatellite solely based on optical navigation. Therefore, it is necessary to keep the distance of the two spacecraft within certain boundaries. This is especially challenging because the employed standard spring mechanism is designed to impart a separation velocity to the picosatellite. A maneuver strategy is developed in the framework of relative orbital elements. The goal is to prevent loss of formation while mitigating collision risk. The main design driver is the performance uncertainty of the release mechanism. The analyzed strategy consists of two maneuvers: the separation itself, and a drift-reduction maneuver of the Berlin Infrared Optical System satellite after 1.5 revolutions. The selected maneuver parameters are validated in a Monte Carlo simulation. It is demonstrated that both the risk of formation evaporation (separation of more than 50 km) as well as the eventuality of a residual drift toward the carrier are below 0.1%. In the latter case, formation safety is guaranteed by a passive safety achieved through a proper relative eccentricity/inclination vector separation.

Notation

a	=	semimajor axis of the carrier satellite, m
e	=	eccentricity of the carrier satellite
e_i	=	delta-v error on the ith tangential component, m/s
f_i	=	simulated performance factor of maneuver i
i	=	inclination of the carrier satellite, deg
k	=	odd natural number
n	=	mean angular motion of the carrier satellite, rad/s
p	=	real number
u	=	mean argument of latitude of the carrier satellite, °
$\boldsymbol{v}$	=	absolute value of velocity vector, m/s
ΔB	=	differential ballistic coefficient, m^2/kg
$\Delta\bullet$	=	finite variation of a quantity
$\delta\boldsymbol{\alpha}$	=	nondimensional relative orbital elements set
$\delta\boldsymbol{e}$	=	nondimensional relative eccentricity vector
$\delta\boldsymbol{i}$	=	nondimensional relative inclination vector
$\delta\lambda$	=	nondimensional relative longitude
$\delta v_R, \delta v_T, \delta v_N$	=	instantaneous velocity changes in local radial–tangential–normal frame, m/s
$\delta\bullet$	=	relative quantity
$\epsilon_{xi}, \epsilon_{yi}, \epsilon_{zi}$	=	simulated errors of the carrier attitude control during maneuver i, rad
θ	=	argument of latitude of the relative ascending node, °
ξ	=	phase change of the relative eccentricity vector, rad
ρ	=	atmospheric density, g/km^3
φ	=	argument of latitude of the relative perigee, °
χ	=	function of the difference between the arguments of latitude of the two maneuvers
Ω	=	right ascension of ascending node of the carrier satellite, deg
ω	=	argument of perigee of the carrier satellite, deg

Presented as Paper AAS-14-414 at the 24th AAS/AIAA Space Flight Mechanics Meeting, Santa Fe, NM, 26–30 January 2014; received 6 May 2014; revision received 27 April 2015; accepted for publication 17 May 2015; published online 13 August 2015.

*Research Engineer, German Space Operations Center.
†Assistant Professor, Department of Aeronautics and Astronautics, Durand Building.

I. Introduction

THIS paper addresses the design of a safe strategy to inject a picosatellite in low Earth orbit after separation from a small satellite carrier. The problem is motivated by the Autonomous Vision Approach Navigation and Target Identification (AVANTI) experiment onboard the Berlin Infrared Optical System (BIROS) [1] spacecraft.

In the recent years, the deployment of small-scale satellites as secondary payloads into low Earth orbit has become more and more common [2–5]. The miniaturization of technology and an increase in the number of educational scientific programs have both contributed to this trend. Within these applications, the launch vehicles are typically equipped with spring-based deployment devices, which provide a linear velocity relative to the carrier that ranges from 0.3 to 2.0 m/s [6]. Because the main purpose of these technology demonstrations is focused on the ejected elements, the separation phase has to quickly and safely establish a certain relative distance, disregarding how different the final dynamics of the two vehicles are. Therefore, the ejection can simply be achieved by imparting the deployment delta-v in flight direction. In this case, the differential drag effect would increase the separation.

In 2010, in the frame of the Prototype Research Instruments and Space Mission technology Advancement (PRISMA) [7] mission, a different application scenario was successfully demonstrated in flight. It involved the separation of two satellites with the aim of performing some formation flying activities. The employed separation mechanism, a three-point system with hooks and clamps kept in locked position by a single wire, was meant to provide a small delta-v (i.e., nominally 0.12 m/s [8]). Moreover, the accuracy of its true performance allowed considering safe relative orbits that intersect the local carrier horizon plane at an along-track separation of the order of 150 m. A further peculiarity of this satellite separation resided in the availability of a GPS receiver on each satellite and of an intersatellite link. Thus, the differential GPS relative navigation could be used to estimate both the deployment delta-v and the residual drift at the end of the separation phase [9].

The problem discussed in this paper presents commonalities with both mentioned categories of applications. On one hand, the BIROS

spacecraft makes use of a spring-based picosatellite orbit deployer (POD) device that provides a large and highly uncertain separation delta-v. On the other hand, the picosatellite release is relevant for the AVANTI experiment, where a noncooperative target (i.e., the ejected picosatellite, which has no onboard actuators for orbit control) is the target of several formation flying activities.

The major challenges of this application stem from the fact that a safe and stable relative motion of the formation has to be established shortly after separation subject to several operational constraints. Nevertheless, the results of this paper allow the extension and generalization of the relative eccentricity/inclination vector separation method [10] to a new class of distributed space systems. Overall, this work proposes an effective way to solve a mission-specific problem that might have relevant applications in future on-orbit servicing and distributed space systems architectures.

The proposed and analyzed guidance and maneuver planning approach is based on the relative eccentricity/inclination vector separation method that was first introduced by Härting et al. [11] for the collocation of geostationary satellites, later applied for long-range rendezvous in low Earth orbits by Montenbruck et al. [12] and finally extended to formation-flying [13] and on-orbit servicing scenarios [14]. Indeed, a safe passively stable relative motion can be established after the release of a picosatellite from a satellite carrier by ensuring the (anti-) parallelism of the relative eccentricity and inclination vectors [12].

A further novelty of the proposed approach is the investigation, at a design level, of how additional relevant operational aspects impact the safety and the feasibility of the guidance plan. Specifically, this study addresses also the distance of the nearest transit of the picosatellite through the local along-track axis, the eventual delay and/or misexecution of the drift-stopping maneuver performed by the carrier, and finally the achievement of a final relative drift with known and safe direction (i.e., which increases the along-track separation), regardless of the uncertainties in the whole control chain.

To deal with such a comprehensive scenario while establishing a desired passively safe stable relative orbit, the preliminary design of the maneuvering strategy is carried out in the relative orbital elements (ROE) framework [15]. These parameters, in fact, are the integration constants of the Hill–Clohessy–Wiltshire equations and provide a direct insight into the geometry and thus into the safety characteristics of the relative motion. By making use of the simple relations between changes in ROE and applied delta-v derived from the inversion of the model of relative dynamics, a nominal scheme of maneuvers to accomplish the separation can be designed. Specifically, it can be shown that a single maneuver cannot establish the parallelism of the relative eccentricity and inclination vectors within the operational constraints of the application under consideration. On the contrary, a double-maneuver strategy can accomplish this task through the tuning of parameters related to the mean along-track separation and to the size of the final relative orbit.

The ultimate validation of the preliminary designed guidance scheme is accomplished through multiple numerical analyses. These take into account several sources of uncertainty that affect the reliability of the nominal plan: 1) the POD delta-v magnitude error due to the spring release mechanism, 2) the BIROS attitude control error, 3) the BIROS maneuver execution error, and 4) the uncertainty in the knowledge of the differential ballistic coefficient. Considering all these uncertainties, a residual drift will remain after the second maneuver. The proposed strategy guarantees that the drift is in the desired direction irrespective of these uncertainties. Before the start of the AVANTI experiment, the residual drift is finally removed by a third maneuver, which is planned on-ground after a dedicated orbit determination of the picosatellite.

In the following, first an overview of the mission with its requirements is provided. Second, the preliminary design of the guidance plan is described, and a baseline scenario compliant with all the relevant operational aspects is selected. Finally, the results of nonlinear Monte Carlo (MC) simulations are presented and discussed, in the attempt to demonstrate the safety and efficiency of the overall methodology.

II. Mission Overview and Requirements

Scheduled for launch in 2016, the BIROS satellite ($60 \times 80 \times 80$ cm, 140 kg) will be operated by DLR, German Aerospace Center. Its primary task, next to several technology demonstration experiments (including AVANTI), will be the observation of wildfires in the frame of the FireBird mission. Together with the similar TET-1 satellite, which was launched in 2012 and is operated by DLR as well, it will form a loose constellation of Earth observation satellites. BIROS is designated for injection into an almost circular sun-synchronous orbit with a local time at the ascending node of 0930 hrs and an orbit height of 515 km. The spacecraft is equipped with a propulsion system and a fuel availability corresponding to circa 20 m/s of delta-v. Half of the fuel is allocated to the AVANTI experiment, whereas the other half is allocated to the primary mission objective.

The AVANTI experiment is intended to demonstrate vision-based, noncooperative autonomous approaches and recede operations of an active small satellite (BIROS) within separations between 10 km and 100 m from a picosatellite ($10 \times 10 \times 10$ cm, 1 kg) making use of angles-only measurements. Gaias et al. [16] provide a description of the experiment objectives and design, whereas details about the onboard relative navigation filter are available in [17]. The picosatellite is originally carried by BIROS and later ejected through a POD deployer after the successful checkout and commissioning of all relevant BIROS subsystems. The AVANTI experiment is intended to start after the BIROS/picosatellite formation has been brought to an initial safe configuration at about 5 km separation with minimal residual drift in the along-track direction. This delicate operational task is solely ground-based and is performed by the Flight Dynamics Services division of the German Space Operations Center (GSOC), which is in charge of the orbit determination and control of the FireBird mission.

The mission profile is characterized by several external constraints that have to be considered during the analysis of a safe separation. First of all, the separation must take place during a ground-station contact, which poses restrictions on the location of the deployment along the orbit and on the separation attitude for proper communication. In particular, the separation will take place at the beginning of a polar ground station contact, and the argument of latitude u_1 for the separation is fixed to 88°. Because a standard POD is adopted, the size of the delta-v imparted to the picosatellite at ejection is 1.41 m/s with a basically unknown dispersion. If oriented in the along-track direction, this corresponds to about 2.8 km semimajor axis difference between the BIROS and picosatellite orbits, which produces an along-track drift of 27 km/orbit or 405 km/day. Because during this phase the only means of navigation information for the picosatellite is radar tracking from ground, with associated latencies of typically 24 h, the risk of formation evaporation would be too high when adopting this conventional separation strategy. In this study, we assume that a mean along-track separation larger than 50 km corresponds to an evaporated formation. This value is derived from the in-flight experience of noncooperative far-range approaches gained by the DLR/GSOC formation reacquisition experiment accomplished in 2011 at the end of the nominal phase of the PRISMA mission [18]. At that time, an intersatellite separation of 55 km was recovered in one week mainly based on two-line-elements information. Nevertheless, because of all the uncertainties that characterize the separation event and control chain, a certain residual drift toward evaporation remains also when employing the guidance scheme proposed here. The radar tracking facility foreseen within the FireBird mission is the Tracking and Imaging Radar (TIRA) station in Germany [19]. According to it, due to the different sizes of the BIROS satellite and the picosatellite, a minimum distance of 5 km is required for TIRA to be able to distinguish the signal from the two spacecraft. Typically, two tracking passes with a spacing of 12 h are necessary for an accurate orbit determination.

Additional geometrical constraints are introduced by the camera employed by the AVANTI experiment. The experience from previous missions suggests that the camera should be able to detect the picosatellite up to a distance of 10 km [20]. The separation scenario

must ensure the visibility of the picosatellite at the start of the AVANTI experiment, considering that the half-field of view of the camera is 6.8 deg horizontally and 9.15 deg vertically.

III. Relative Motion Description

The relative motion is parameterized by this set of dimensionless relative orbital elements (ROEs):

$$\delta\alpha = \begin{pmatrix} \delta a \\ \delta\lambda \\ \delta e_x \\ \delta e_y \\ \delta i_x \\ \delta i_y \end{pmatrix} = \begin{pmatrix} \delta a \\ \delta\lambda \\ \delta e\cos\varphi \\ \delta e\sin\varphi \\ \delta i\cos\theta \\ \delta i\sin\theta \end{pmatrix} = \begin{pmatrix} (a-a_d)/a_d \\ u-u_d+(\Omega-\Omega_d)\cos i_d \\ e\cos\omega - e_d\cos\omega_d \\ e\sin\omega - e_d\sin\omega_d \\ i-i_d \\ (\Omega-\Omega_d)\sin i_d \end{pmatrix} \tag{1}$$

where a, e, i, Ω, and M denote the classical Keplerian elements, and $u = M + \omega$ is the mean argument of latitude. The subscript "d" labels the deputy spacecraft of the formation, which plays the role of the maneuverable carrier satellite (BIROS) and defines the origin of the local radial–tangential–normal (RTN) frame. The quantities $\delta\boldsymbol{e} = (\delta e\cos\varphi, \delta e\sin\varphi)^T$ and $\delta\boldsymbol{i} = (\delta i\cos\theta, \delta i\sin\theta)^T$ define the dimensionless relative eccentricity and inclination vectors, where φ and θ respectively represent the perigee and ascending node of the relative orbit [12]. In the following, their magnitudes are shortly quoted as $\delta e = \|\delta\boldsymbol{e}\|$ and $\delta i = \|\delta\boldsymbol{i}\|$, whereas the subscript is dropped, meaning that all the absolute orbital quantities appearing in the equations belong to the carrier satellite.

Under the assumptions of the Hill–Clohessy–Wiltshire (HCW) equations [21], the quantities $a\delta e$ and $a\delta i$ provide the amplitudes of the in-plane and out-of-plane relative motion oscillations (see Fig. 1), whereas relative semimajor axis $a\delta a$ and relative mean longitude $a\delta\lambda = a(\delta u + \delta i_y\cot i)$ provide mean offsets in the radial and along-track directions, respectively [10,22]. Moreover, if no orbital perturbations are considered, the only ROE that varies with time is the relative mean longitude according to

$$\delta\lambda(u) = -1.5(u-u_0)\delta a_0 + \delta\lambda_0 \tag{2}$$

According to the model of the relative dynamics just introduced, the instantaneous dimensional variations of the ROE caused by an impulsive maneuver (or an instantaneous velocity change) at the mean argument of latitude u_M are given by

$$\begin{aligned} a\Delta\delta a &= +2\delta v_T/n \\ a\Delta\delta\lambda &= -2\delta v_R/n \\ a\Delta\delta e_x &= +(\delta v_R/n)\sin u_M + 2(\delta v_T/n)\cos u_M \\ a\Delta\delta e_y &= -(\delta v_R/n)\cos u_M + 2(\delta v_T/n)\sin u_M \\ a\Delta\delta i_x &= +(\delta v_N/n)\cos u_M \\ a\Delta\delta i_y &= +(\delta v_N/n)\sin u_M \end{aligned} \tag{3}$$

which, as explained in [22], can be equivalently derived either from the Gauss variational equations or from the HCW solution at the time when $u = u_M$. In Eq. (3), n indicates the mean motion of the carrier, and the delta-v is expressed in the RTN frame:

$$\delta\boldsymbol{v} = (\delta v_R, \delta v_T, \delta v_N)^T \tag{4}$$

Before the release of the picosatellite, the relative state $a\delta\alpha$ is null. Then, if a single separation maneuver is executed at the mean argument of latitude u_1, the following ROE variations can be established at $u = u_1$:

$$\begin{cases} na\Delta\delta a = 2\delta v_T \\ na\Delta\delta\lambda = -2\delta v_R \\ na\Delta\delta e = \sqrt{\delta v_R^2 + 4\delta v_T^2} \\ \tan(u_1-\xi) = \frac{\delta v_R}{2\delta v_T} \\ na\Delta\delta i = |\delta v_N| \\ \tan(u_1) = \frac{\Delta\delta i_y}{\Delta\delta i_x} \end{cases} \tag{5}$$

where ξ denotes the obtained phase angle of the relative eccentricity vector.

As mentioned previously, the location of the first separation maneuver is fixed by the need of performing it during a given ground contact. Furthermore, the magnitude is fixed by making use of a POD device with a fixed δv of 1.41 m/s. On the other hand, the direction of the impulse is freely selectable. This poses the following constraint on the magnitude of the separation maneuver:

$$\delta v = \|\delta\boldsymbol{v}\| = \sqrt{\delta v_R^2 + \delta v_T^2 + \delta v_N^2} \tag{6}$$

and the number of effective degrees of freedom of the problem is reduced so that one can satisfy only two of the conditions of Eq. (5).

By analyzing the obtainable relative motion within the requirements of this application scenario, it can be proven that if $\delta v_T = 0$, the established relative motion is characterized by $\delta\boldsymbol{e}^T\delta\boldsymbol{i} = 0$; see Eq. (3). In other words, radial and cross-track maneuvers at the same location produce perpendicular relative eccentricity and inclination vectors. Thus, the minimum separation in the radial–normal (R–N) plane is null, which is not acceptable for safety reasons in the presence of along-track position uncertainties [13]. In contrast, if $\delta v_T \neq 0$ and $\delta v_R \neq 0$, the phase of $\delta\boldsymbol{e}$ can be changed. Unfortunately this change is not as much needed to obtain (anti-) parallel relative eccentricity/inclination vectors after one maneuver.

It is emphasized that, to avoid a collision, it is necessary to establish a certain drift in the relative motion through the first separation maneuver (i.e., δv_T must be $\neq 0$). In this case, in fact, the first passage of the deputy satellite across the along-track axis will occur after some separation is built up.

In conclusion, because it is not possible to achieve a bounded passively safe orbit through a single separation maneuver, a second maneuver is strictly required, as addressed in the following section.

A. Separation Preliminary Design: Double-Maneuver Scheme

The analytical form of the general expression of the in-plane double-pulse maneuvers' scheme, for whatever aimed final conditions, as a function of the mean arguments of latitude of the two maneuvers is given in [15] [i.e., Eq. (12)]. Nevertheless, this expression is quite complicated and does not allow an immediate geometrical insight into the geometry of the relative motion. At a preliminary stage, Eq. (2.42) of [10] can be used:

$$\begin{aligned} \delta v_{R1} &= \frac{na}{2}\left(-\frac{\Delta\delta\lambda^*}{2} + \Delta\delta e\,\sin(u_1-\xi)\right) \\ &\quad -\frac{na}{2}\chi(\Delta\delta a - \Delta\delta e\,\cos(u_1-\xi)) \\ \delta v_{T1} &= \frac{na}{4}(+\Delta\delta a + \Delta\delta e\,\cos(u_1-\xi)) \\ &\quad -\frac{na}{4}\chi\left(\frac{\Delta\delta\lambda^*}{2} + \Delta\delta e\,\sin(u_1-\xi)\right) \\ \delta v_{R2} &= \frac{na}{2}\left(-\frac{\Delta\delta\lambda^*}{2} - \Delta\delta e\,\sin(u_1-\xi)\right) \\ &\quad +\frac{na}{2}\chi(\Delta\delta a - \Delta\delta e\,\cos(u_1-\xi)) \\ \delta v_{T2} &= \frac{na}{4}(+\Delta\delta a - \Delta\delta e\,\cos(u_1-\xi)) \\ &\quad +\frac{na}{2}\chi\left(\frac{\Delta\delta\lambda^*}{2} + \Delta\delta e\,\sin(u_1-\xi)\right) \end{aligned} \tag{7}$$

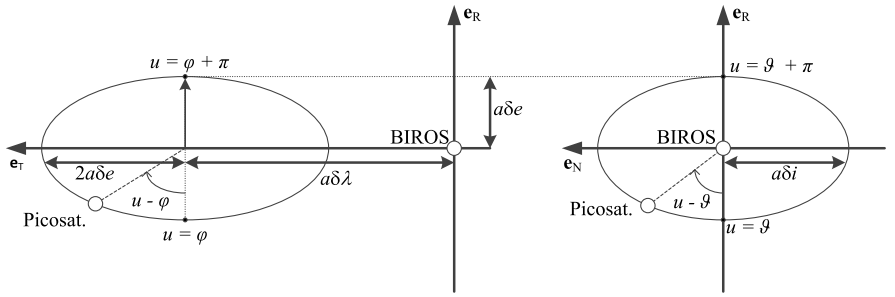

Fig. 1 Sketch of ROEs and their relation to the relative motion in the RTN frame.

with

$$\chi = \frac{\sin \Delta u}{\cos \Delta u - 1} \quad \Delta u = u_2 - u_1 \quad \xi = \arctan\left(\frac{\Delta\delta e_y}{\Delta\delta e_x}\right) \tag{8}$$

Equation (7) provides an analytical expression of the double-impulse in-plane scheme to achieve a prescribed total variation of $\Delta\delta a$, $\Delta\delta\boldsymbol{e}$, and $\Delta\delta\lambda^*$. This expression is very useful because, in our application, the initial relative state is null, and the total aimed variation coincides with the final aimed relative state:

$$\Delta\delta\bullet = \delta\bullet_F \quad \text{and} \quad \varphi_F = \xi \tag{9}$$

The simple and practical form of Eq. (7) has been obtained by neglecting that $\delta\lambda$ changes over time when the relative semimajor axis after the first maneuver δa_1 is not null, according to Eq. (2). Therefore, the truly obtainable relative longitude at the final time $\delta\lambda_F = \Delta\delta\lambda$ will not exactly amount to $\Delta\delta\lambda^*$. The required correction is later on discussed through Eq. (14). Nevertheless, at a preliminary design stage, Eq. (7) is acceptable and allows achieving a much simpler expression of the in-plane delta-v.

When dealing with the in-orbit release of a satellite, Eq. (7) must be complemented with the out-of-plane equations. The passive safety constraint of final (anti-) parallelism of the relative eccentricity/inclination vectors, in fact, couples back to the impulsive reconfiguration problem.

In the following, the remaining specific requirements of the separation problem are listed and discussed, together with their geometrical interpretation in the ROE space. In Fig. 2, all the final desired quantities, which are the parameters that appear in Eq. (7), are marked in black. The other quantities represent the intermediate values obtained during the execution of a double-impulse maneuvering scheme.

The following features characterize this application scenario. First of all, the location of the first maneuver u_1 is fixed and known because the deployment has to occur during the aforementioned ground contact. Consequently, the phase of the relative inclination vector after the first maneuver θ is also fixed. This is shown in Fig. 2 by the dotted light gray segment in the $\delta\boldsymbol{i}$ plane. Note that $u = u_1 = \theta_F$, assuming that $\delta v_{N1} > 0$ without loss of generality. Furthermore, to achieve passive safety, it has to be imposed that the phase of the final $\delta\boldsymbol{e}$, ξ is equal to θ_F. This is shown in Fig. 2 by the dotted light gray segment in the first and third quadrants of the $\delta\boldsymbol{e}$ plane. Thus, in a general case, one can impose $\xi = \theta_F + \eta$, where the service parameter η can only assume the values of 0 or π. The aim is to establish a final stable relative orbit; thus, $\delta a_F = 0$. This implies that all terms in $\Delta\delta a$ in Eq. (7) vanish. Equation (7) is defined for $\Delta u \neq 0$ or $\neq 2\pi$. In all other cases, χ weights the effect of the maneuvers' spacing on the final four in-plane delta-v expressions. In the special case of k odd number and $\Delta u = k\pi$, the second part of Eq. (7) vanishes. As a result, the delta-v expressions are characterized by a symmetrical form. Moreover, in these particular locations of the second maneuver, the effect of the second out-of-plane maneuver can only change the magnitude of $\delta\boldsymbol{i}$, and not the phase θ_F, whenever δv_{N2} is nonzero. This is marked by the gray arrows in the left side of Fig. 2. As already mentioned previously, the first maneuver is accomplished by the deployment device; thus, its magnitude is constrained to δv. This introduces a relationship on the three RTN components and, consequently, on the achievable $\Delta\delta e$, $\Delta\delta\lambda^*$, and $\Delta\delta i$.

By taking into account the aforementioned requirements, the delta-v expressions of Eq. (7) simplify to

$$\begin{aligned}
\delta v_{R1} &= -\frac{na}{4}(\Delta\delta\lambda^*) \\
\delta v_{T1} &= \pm\frac{na}{4}(\Delta\delta e) \\
\delta v_{R2} &= -\frac{na}{4}(\Delta\delta\lambda^*) \\
\delta v_{T2} &= \mp\frac{na}{4}(\Delta\delta e)
\end{aligned} \tag{10}$$

because $u_1 = \xi$. The signs of Eq. (10) are determined by fixing η (i.e., the final $\delta\boldsymbol{e}/\delta\boldsymbol{i}$ configuration) and by the sign of $\Delta\delta\lambda^*$, which is

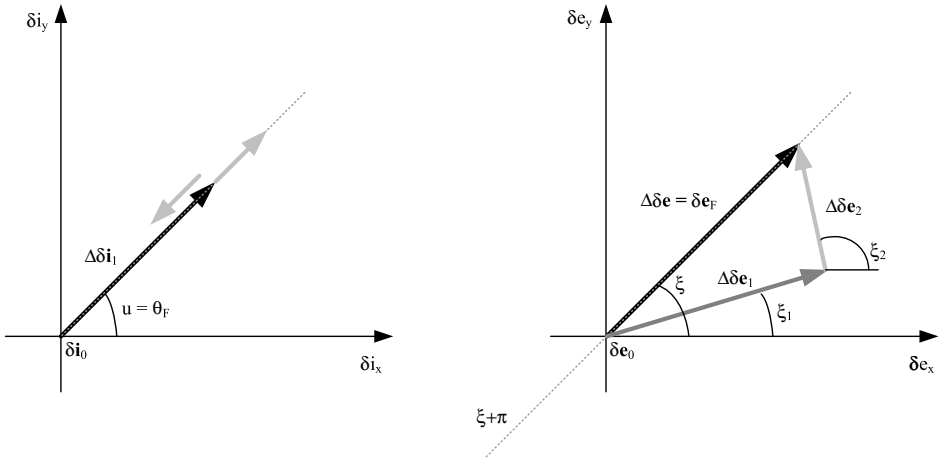

Fig. 2 Sketch in the ROE space of the maneuvering scheme of Eq. (7) to achieve passive safety.

equivalent to the sign of $\delta\lambda_F$ (i.e., picosatellite leading or following the carrier).

At conclusion of this preliminary design section, the simple delta-v expression of Eq. (10) has been achieved. This is the result of imposing the satisfaction of the separation final conditions (i.e., passively safe bounded relative orbit) through only two maneuvers. Moreover, the operational requirement on the location of the picosatellite ejection has been included, together with the two design assumptions of $\delta v_{N1} > 0$ and $\chi = 0$. At this point, the remaining degrees of freedom of the separation problem are two among δe_F, δi_F, and $\delta\lambda_F$ together with the spacing between the maneuvers (i.e., the number of half-revolutions k). These parameters are fixed as soon as an aimed final orbit is identified. Therefore, the next section deals with the identification of such a nominal baseline to cope with some operative aspects of crucial importance in realistic scenarios.

B. Baseline Identification in Compliance with the Operative Constraints

This section discusses how some operative constraints impact the degrees of freedom of the preliminary design formulation. The outcome is the identification of feasible baselines for the aimed relative orbit. An analysis and verification of their robustness with respect to system uncertainties is accomplished afterward.

Table 1 lists the main operative constraints that are involved in the in-orbit release of a satellite, as explained previously. Constraints safety 1 and visibility 1 determine the domain of the aimed relative mean longitude, that is the mean satellite separation in tangential direction. Safety constraint 2 determines the parallel or antiparallel $\delta\boldsymbol{e}/\delta\boldsymbol{i}$ configuration (i.e., η). In particular, if the picosatellite is released so that, at the end of the separation, it leads the carrier in flight direction, an instantaneous negative radial delta-v must be imparted (i.e., $\delta v_{R1} < 0$). Therefore, to avoid an immediate crossing of the local along-track axis, the semimajor axis of the picosatellite shall be reduced (i.e., $\delta v_{T1} < 0$) to drift toward positive along-track separations. This combination of signs in Eq. (10) is obtained with $\eta = \pi$ in Eq. (7) because $\xi = \theta_F + \eta$. Thus, the final aimed relative orbit must have antiparallel relative $\boldsymbol{e}/\boldsymbol{i}$ vectors.

The safe complementary situation (i.e., picosatellite released to follow the carrier) requires $\delta v_{R1} > 0$ and a positive drift (i.e., $\delta v_{T1} > 0$). According to the chosen maneuvering scheme, this is obtained if $\eta = 0$, thus establishing a parallel configuration.

The choice of having picosatellite leading/following BIROS can be taken by considering the safety constraints 3 and 4. They address the natural effect of the differential drag. In this application, the ballistic drag coefficient of the picosatellite is greater than that of BIROS; thus, its orbit lowers faster, producing a drift at a relative level (note that, in this paper, the ballistic drag coefficient $B = C_D A/m$ is used instead of its inverse quantity the ballistic coefficient to be in line with other satellite work). Specifically, if the picosatellite is leading the carrier in flight direction, the natural drift tends toward larger separations. In the opposite situation, the picosatellite will tend to come back toward the carrier. The tradeoff between evaporation or proximity shall take into account safety constraint 4 as well. According to it, any dangerous situation before the accomplishment of the second maneuver shall be avoided. This is motivated by the fact that a single maneuver is not able to establish passive safety (see previous sections).

Therefore, to satisfy the first four safety requirements, according to this scenario, a final configuration with the picosatellite leading the carrier in positive tangential direction is to be preferred. Consequently, $\Delta\lambda_F > 0$ and $\eta = \pi$. The range of feasible sizes of the aimed relative orbit are derived from the remaining constraints of Table 1.

Safety constraint 6 requires that the direction of the drift is unequivocally defined, disregarding the size of execution error of the first maneuver. Thus, by considering an error $\tilde{e}$ of magnitude 0.141 m/s (i.e., 10% of the total magnitude δv), the delta-v in the tangential direction must produce a negative drift in any case. This implies

$$|\delta v_{T1}| = \frac{na}{4}\delta e_F > \tilde{e} \rightarrow a\delta e_{\min} = 511.25 \text{ m} \tag{11}$$

for the carrier at an orbit altitude of 515 km.

The same error consideration applied in the normal component of the delta-v impacts the truly obtainable magnitude of the relative inclination vector. This is referred to as safety constraint 7 in Table 1 and fixes the margin equal to $\tilde{e}/n$ [i.e., 127.81 m at the same orbit height of Eq. (11)], where n is the carrier mean motion.

The minimum size of the stable final relative orbit is also limited by passive safety considerations (i.e., safety constraint 5) that ask for a minimum R–N distance of 100–150 m. By merging all these requirements, the lower bounds reported in Table 2 are obtained.

Finally, the maximum size of the relative orbit is constrained by the field of view (FOV) of the camera (i.e., visibility constraints 2 and 3). The worst case scenario occurs at the minimum allowed mean relative longitude value (i.e., $a\delta\lambda_F = 5000$ m). By making use of Eq. (3) [20], and by neglecting the correction due to curvature, the following limits are identified:

$$\delta e_F < \tan(6.8^\circ)|\delta\lambda_F| \qquad \delta i_F < \tan(9.15^\circ)|\delta\lambda_F| \tag{12}$$

and the subsequent values are also collected in Table 2.

It is emphasized that the three final magnitudes $\delta\lambda$, δe, and δi cannot be chosen independently, due to the constraint on the magnitude of the first maneuver. Moreover, in Eq. (10), the $\Delta\delta\lambda^*$ value appears instead of the true $\delta\lambda_F$, due to the simplifications introduced by Eq. (7).

Both these points suggest choosing δe and δi as design parameters, in their domains of feasibility. Consequently, the value of the radial component of the first delta-v is given by

Table 2 Admissible sizes of the final relative orbit

Aimed ROE	Minimum magnitude, m	Maximum magnitude, m
$a\delta\lambda$	5000	10,000
$a\delta e$	512	596
$a\delta i$	278	805

Table 1 Meaningful operative constraints for the in-orbit satellite release

Constraint	Identifier	Description	Consequence
Safety	1	TIRA tracking capability	$\lvert a\delta\lambda_F\rvert \geq 5000$ m
Safety	2	First cross of the along-track axis	Given $\delta\lambda_F$ and $\chi = 0$, fixes η
Safety	3	Effect of differential drag	Choice of the direction of $\delta\lambda_F$
Safety	4	Delay of second maneuver	No collision before passive safety achievement
Safety	5	Passive safety	Given η, minimum size of δe_F and δi_F
Safety	6	Sign of δa after first maneuver	$\lvert\delta v_{T1}\rvert$ greater than spring error
Safety	7	Truly obtainable $a\delta i$	aimed $\delta i > (\delta i_{\min} + \text{margin})$
Visibility	1	Picosatellite camera detectability	$\lvert a\delta\lambda_F\rvert \leq 10,000$ m
Visibility	2	Camera FOV in R direction	$a\delta e_{\max} < 596$ m at $a\delta\lambda_F = 5000$ m
Visibility	3	Camera FOV in N direction	$a\delta i_{\max} < 805$ m at $a\delta\lambda_F = 5000$ m

$$\delta v_{R1} = -\sqrt{\delta v^2 - \delta v_{T1}{}^2 - \delta v_{N1}{}^2} \tag{13}$$

and $\Delta\delta\lambda^*$ is then computed using the first of Eq. (10).

This obtained value influences the choice of k, so that the final $\delta\lambda_F$ is in its domain of feasibility. The relationship between the obtained relative mean longitude and $\Delta\delta\lambda^*$ of Eq. (7) is provided by

$$\delta\lambda_F = -1.5(k\pi)\delta a_1 + \Delta\delta\lambda^* \tag{14}$$

where $\delta a_1 = (2/n)\delta v_{T1}$. Therefore, once fixed δv_{R1} (i.e., fixed δe and δi), k can be chosen as the odd natural number comprised in

$$-\frac{5000 - \Delta\delta\lambda^*}{1.5\pi\delta a_1} \le k \le -\frac{10,000 - \Delta\delta\lambda^*}{1.5\pi\delta a_1} \tag{15}$$

Some remarks can be added when dealing with the final selection of the baseline (i.e., aimed δe and δi). Visibility constraints 2 and 3 can be handled as soft constraints because they become less critical when the separation increases. Both differential drag and the choice of a bigger k contribute to this. The magnitude of δi can be small (coherently with its domain) to avoid further consumption of delta-v due to a second cross-track burn. Moreover, this allows allocating more delta-v to the tangential and radial components of the first maneuver, which is fruitful for safety constraint 6 and for establishing faster a certain separation. Visibility constraint 1 could also be softened because later corrections can be accomplished before switching to visual-based relative navigation (at the cost of further delta-v consumption).

An example of feasible baseline can be obtained by choosing the following values:

$$\begin{aligned} a\delta e_F &= 590 \text{ m} \\ a\delta i_F &= 400 \text{ m} \end{aligned} \tag{16}$$

leading to these nominal delta-v magnitudes:

$$\begin{aligned} \delta\boldsymbol{v}_1 &= (\delta v_{R1}, \delta v_{T1}, \delta v_{N1})^T \\ &= (-1.329250, -0.162718, 0.441269)^T \text{ m/s} \\ \delta\boldsymbol{v}_2 &= (\delta v_{R2}, \delta v_{T2}, \delta v_{N2})^T \\ &= (-1.329250, +0.162718, 0.0)^T \text{ m/s} \end{aligned} \tag{17}$$

The admissible values of k to satisfy Eq. (15) are [1,3]. It is emphasized that, because the delta-v do not depend on this choice [see Eq. (10)], the same delta-v plan remains valid in the case that any anomaly prevented executing the second maneuver. Besides, a delay in the execution of such maneuver causes the aimed $\delta\lambda_F$ to increase according to Eq. (14).

Figure 3 shows the nominal relative trajectory obtained with $k = 3$ in the RTN frame with the BIROS satellite in the origin. At this level of the analysis, no disturbances are included in the ROE propagation. The thin lines in the R–N, radial–tangential, and tangential–normal (T–N) views define the area of the FOV of the camera mounted on the BIROS spacecraft, whereas the solid gray line denotes the relative trajectory before the second maneuver, and the solid black line denotes the relative trajectory after the second maneuver.

Before dealing with the verification of the chosen baseline with respect to system's uncertainties, a final design problem needs to be addressed. It concerns the sign of the final relative drift when the executed delta-v differ from the nominal commanded ones. This topic is relevant because one cannot estimate the truly executed first impulse before accomplishing the second maneuver.

Because the drift is linked to the tangential components of the delta-v, at a design level, it can be assumed that no error is accomplished on the radial and normal components of Eq. (17). When the truly executed first tangential maneuver is given by

$$\delta v_{T1}^* = \delta v_{T1} + e_1 \tag{18}$$

a possible critical situation can arise if e_1 reduces the magnitude of δv_{T1}^* (i.e., $e_1 > 0$). In this case, the second tangential maneuver would produce a drift reversal, resulting in a drift of the picosatellite toward the carrier. Because the delta-v values are computed according to Eq. (10), increasing the baseline value of $\Delta\delta e$ does not remove this problem.

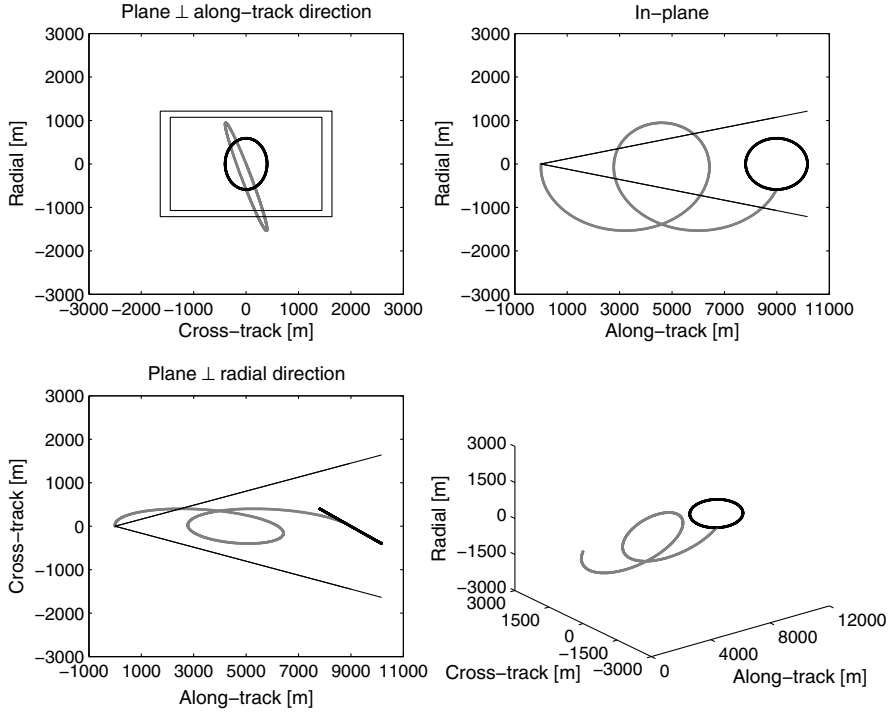

Fig. 3 Example of the feasible baseline of Eq. (16) with delta-v of Eq. (17).

A mitigation of this issue can be achieved by commanding the following nominal tangential delta-v for the second maneuver instead:

$$\delta v_{T2}^{*} = \delta v_{T2} + e_2 - |p| \tag{19}$$

where the parameter p has to be sized to properly determine the strength of the drift reduction. The error in the tangential component of the second maneuver e_2 increases the magnitude of the drift reduction whenever $e_2 > 0$.

This approach exploits the particular structure of this separation design formulation. It can be shown, in fact, that given the two maneuvers spaced by $k\pi$ and having $|\delta v_{R1}| = |\delta v_{R2}|$ [see Eq. (10)], the final phase of the relative eccentricity vector ξ remains the same whatever value of δv_{T1}^{*} and δv_{T2}^{*} are performed. Moreover, the final magnitude of the relative eccentricity vector is given by

$$a\delta e_F^{*} = \frac{1}{n}\sqrt{4({\delta v_{T1}^{*}}^2 + {\delta v_{T2}^{*}}^2 - 2\delta v_{T1}^{*}\delta v_{T2}^{*})} \tag{20}$$

Hence, the parameter p can be chosen such that the sign of the final relative semimajor axis δa_F^{*} is negative even with the greatest under performance of the POD device. At the same time, p is limited by the need to perform at least some drift reduction. These two statements can be formalized as

$$\begin{cases} \delta v_{T2} - e_2 - |p| > 0 \rightarrow \delta v_{T2}^{*} > 0 \\ \delta v_{T2} + e_2 - |p| \leq |\delta v_{T1}| - e_1 \rightarrow \delta a_F^{*} < 0 \end{cases} \tag{21}$$

which lead to the following design range for p:

$$e_1 + e_2 \leq |p| < \frac{na}{4}\delta e_F - e_2 \tag{22}$$

having used $\delta v_{T2} = |\delta v_{T1}| = na\delta e_F/4$.

To conclude this section, the choice of the aimed final relative orbit shall be accomplished by selecting the values ($a\delta e_F$, $a\delta i_F$, p) that allow satisfying all the constraints considered thus far. Moreover, one should verify that the final $a\delta e_F^{*}$ from Eq. (20) meets the passive safety requirement (i.e., safety constraint 5 in Table 1), despite the presence of p. Finally, the case of overperformance of the POD device shall be taken into account. The maximum drift imparted by the first maneuver shall not bring to evaporation, having weakened the drift reduction through p.

IV. Monte Carlo Simulation

To validate the risk of the planned maneuver strategy, MC simulations have been performed in the ROE framework. It should be noted that all simulation runs were executed generating 100,000 samples, but only 1000 are plotted for readability.

The simulation uses the dispersion parameters discussed later. The uncertainty of the POD mechanism is unknown; hence, a pessimistic dispersion with a standard deviation of 10% of the overall delta-v is assumed. This is expressed by multiplying the first maneuver by a factor f_1, which has a mean value of 1 and a standard deviation of 0.1. The execution accuracy of the BIROS propulsion system is unknown at this stage. Similar to the POD mechanism, a dispersion of 5% is assumed. This is expressed by multiplying the second maneuver by a factor f_2, which has a mean value of 1 and a standard deviation of 0.05. It is noted that it will be possible to accurately calibrate the BIROS thrusters during the commissioning phase; hence, this value might change at a later stage. The BIROS satellite is known to have an attitude control accuracy of 30 arcsec. This is expressed by multiplying both maneuvers by a rotation matrix for infinitesimal angles, where the quantities ϵ_x, ϵ_y, and ϵ_z have a mean value of 0 and a standard deviation of 30". The simulated delta-v δv_{Ri}^{s} for maneuvers $i = 1, 2$ are obtained by

$$\begin{pmatrix} \delta v_{Ri}^{s} \\ \delta v_{Ti}^{s} \\ \delta v_{Ni}^{s} \end{pmatrix} = f_i \begin{pmatrix} 1 & \epsilon_{zi} & -\epsilon_{yi} \\ -\epsilon_{zi} & 1 & \epsilon_{xi} \\ \epsilon_{yi} & -\epsilon_{xi} & 1 \end{pmatrix} \begin{pmatrix} \delta v_{Ri} \\ \delta v_{Ti} \\ \delta v_{Ni} \end{pmatrix} \tag{23}$$

The effect of the differential drag on the relative mean longitude and relative semimajor axis can be computed as [10]

$$a\delta\lambda(t) = \frac{3}{4n^2}\Delta B\rho v^2(u(t) - u_0)^2 \tag{24}$$

$$a\delta a(t) = -\frac{1}{n^2}\Delta B\rho v^2(u(t) - u_0) \tag{25}$$

Considering the physical properties of BIROS (cross section of 0.8×0.6 m at nominal attitude, weight of 140 kg) and the picosatellite (cross section of 0.1×0.1 m, weight of 1 kg) with an assumed atmospheric density of $\rho = 1$ g/km^3 and a drag coefficient of $c_d = 2.3$, the relative ballistic drag coefficient can be determined as $\Delta B = 0.0151$ m^2/kg. Nevertheless the atmospheric density, the true effective cross section (due to attitude maneuvers), and the true weight of the satellites (e.g., due to fuel consumption) are difficult to predict. Hence, an ad hoc uncertainty of the differential drag with standard deviation of 20% is applied in the Monte Carlo simulations.

Using the baseline maneuvers determined previously [see Eq. (17)] and assuming a maximum under performance of 3σ for both maneuvers, a reduction value of $p = 0.0732231$ m/s is determined. A first Monte Carlo simulation was executed without including the effect of differential drag to verify if the final relative semimajor axis $a\delta a$ can assume a positive value, which would result in the satellites drifting toward each other. As can be seen in Fig. 4, in none of the cases $a\delta a$ is positive. In the following figures, each dot represents one sample of the simulation. In Figs. 4–6, the remaining relative semimajor axis after the second maneuver is plotted against the mean separation in tangential direction. The left plots show the situation directly after the second maneuver, whereas the right ones show the

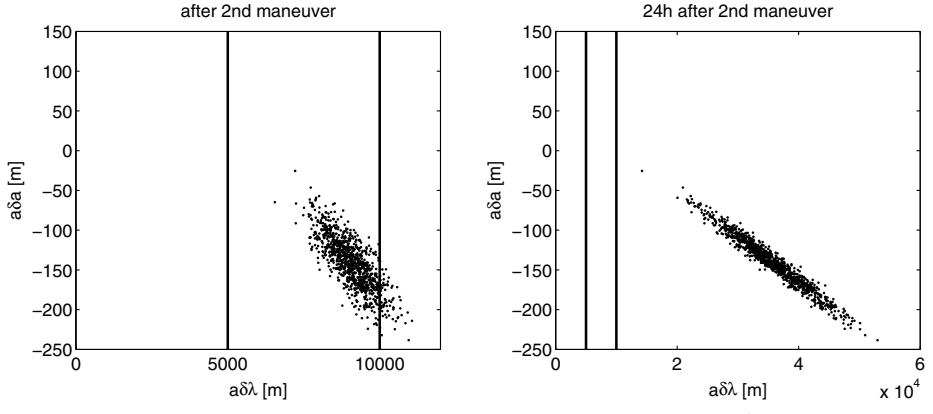

Fig. 4 Residual $a\delta a$ in dependence of mean tangential separation ($p = 0.0732231$ m/s, no differential drag).

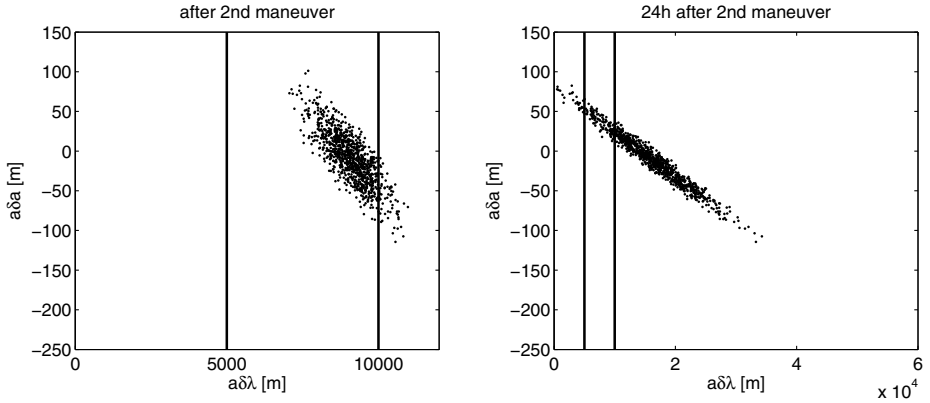

Fig. 5 Residual $a\delta a$ in dependence of mean tangential separation ($p = 0$ m/s, drag included).

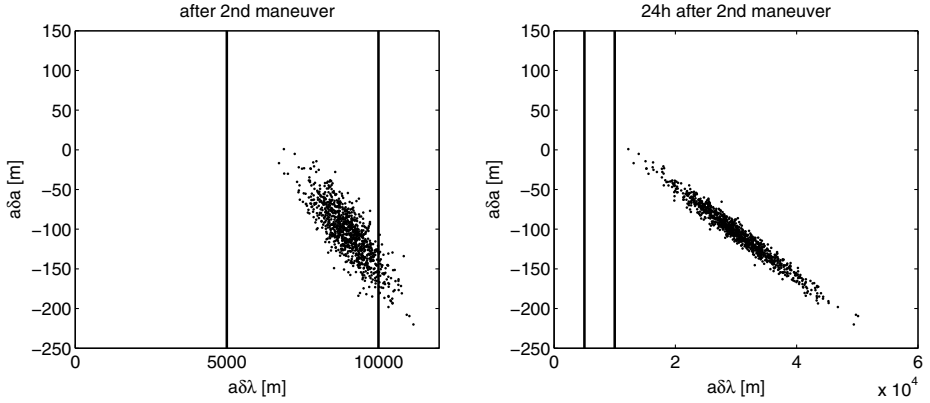

Fig. 6 Residual $a\delta a$ in dependence of tangential separation ($p = 0.055$ m/s, drag included).

development 24 h later, when the third maneuver is about to be performed. The bold lines at $a\delta\lambda = 5000$ m and $a\delta\lambda = 10,000$ m show the thresholds of separability by radar tracking and of visibility by the BIROS onboard camera.

A second simulation run was executed with the differential drag effect taken into account and the reduction value p set to 0 to demonstrate the effect of the differential ballistic coefficient on the remaining drift. As can be see in Fig. 5, in more than 40% of the cases, $a\delta a$ is positive. In about 3.6% of the cases, the drift induced by the relative semimajor axis has led to a reduction of the mean tangential separation to less than 5000 m, and in 0.3% of the cases, the BIROS satellite even passed the picosatellite in tangential direction. This undesired approach leads to the two spacecraft being indistinguishable by radar tracking and renders relative orbit determination impossible.

This demonstrates that the differential drag effect alone is not enough to prevent an approach of the satellites, and a reduction of the tangential component of the second maneuver is necessary. The parameter p has to be tuned such that the likelihood of an approach of the satellites (i.e., $a\delta a > 0$), as well as that of an evaporation of the formation, is minimized. A threshold of 50 km is defined as formation evaporation because, below that distance, the formation can be recovered without too much effort from ground. Table 3 shows the probabilities of an approaching drift and formation evaporation for a selected range of p. The probability is computed by the number of events ($a\delta a > 0$ or $a\delta\lambda > 50$ km) divided by the total number of simulation runs. It is not possible to eliminate both the risks, but with a value of $p = 0.055$ m/s, a minimum of the combined risk is found.

As stated previously, a close approach of the satellites cannot be excluded with $p = 0.055$ m/s. This is confirmed by Fig. 6, which shows that a very small number of cases with $a\delta a > 0$ remains. Hence, it needs to be verified that the established passive safety is sufficient to avoid a collision in case of an approach of the two spacecraft in tangential direction. The magnitudes of the relative eccentricity $a\delta e$ and relative inclination $a\delta i$ are shown in Fig. 7. The limits for safety (150 m in both radial and normal) and visibility (596 m in radial, 805 m in normal) are indicated in the plot. It can be seen that, in rare (0.02%) cases, the limits for visibility are violated, but the requirement on the minimum magnitude is always fulfilled.

To verify the passive safety, this magnitude information has to be complemented with the phasing of the relative $\boldsymbol{e/i}$ vectors. This allows to compute the minimum distance in the plane identified by R and N. Under the assumption of $a\delta a = 0$, the minimum separation perpendicular to the flight direction is defined as [10]

$$\delta r_{\mathrm{nr}}^{\min} = \frac{\sqrt{2}a|\delta\boldsymbol{e}\cdot\delta\boldsymbol{i}|}{(\delta e^2 + \delta i^2 + |\delta\boldsymbol{e} + \delta\boldsymbol{i}|\cdot|\delta\boldsymbol{e} - \delta\boldsymbol{i}|)^{1/2}} \tag{26}$$

This equation shows the importance of parallel or antiparallel relative eccentricity and inclination vectors due to the scalar product of those vectors. In Fig. 8, the minimum cross-track distance is

Table 3 Selection of the reduction value p for the nominal guidance plan of Eq. (17)

p, m/s	$a\delta a > 0$, m	$a\delta\lambda > 50$, km
0.00	41.76%	<0.01%
0.01	22.59%	<0.01%
0.02	9.53%	<0.01%
0.03	3.16%	<0.01%
0.04	0.83%	<0.01%
0.05	0.17%	0.01%
0.055	0.07%	0.03%
0.06	0.03%	0.08%
0.07	0.01%	0.36%
0.08	<0.01%	1.31%

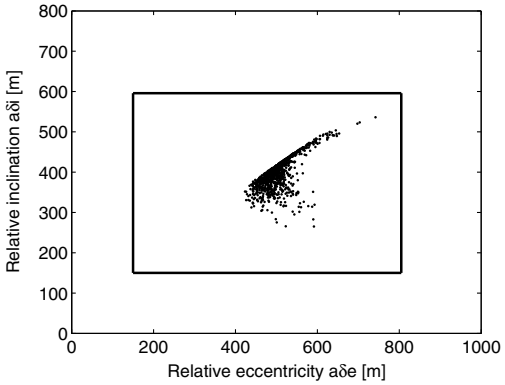

Fig. 7 Relative eccentricity $a\delta e$ and inclination $a\delta i$ after second maneuver.

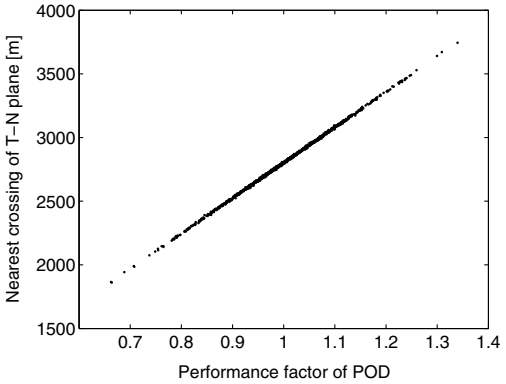

Fig. 9 Nearest crossing of the T–N plane.

plotted as a function of the residual $a\delta a$. As stated previously, Eq. (26) is valid for $a\delta a = 0$, but in most cases, $a\delta a$ is negative; thus, the picosatellite is drifting toward greater separations. Only in the rare event of severe underperformance of the release mechanism, $a\delta a$ is close to 0. In these cases, $\delta r_{\mathrm{nr}}^{\mathrm{min}}$ is about 150 m (see Fig. 8), which means that the passive safety of the formation is guaranteed.

Finally, it has to be verified that a collision risk before the execution of the second maneuver can be ruled out. In case of a severe underperformance of the spring mechanism, the two spacecraft could approach after one revolution if not enough tangential separation has been built up. Therefore, the tangential separation at the nearest crossing of the T–N plane is examined. Figure 9 shows that distance as a function of the performance factor f_1 of the separation mechanism. It can be seen that the behavior is almost linear, but even in the case of a 3σ underperformance ($f_1 < 0.7$), the tangential separation is still larger than 1600 m, and no collision risk exists.

To conclude, the results of the robustness analysis of the baseline of Eq. (17) with the second tangential impulse reduced by a factor $p = 0.055$ m/s demonstrate that all the safety requirements are met, despite the uncertainties taken into account. At completion of the second maneuver, in fact, the residual relative semimajor axis is not positive with a mean along-track separation suitable for radar tracking observations (i.e., Fig. 6); passive safety is guaranteed by always acceptable values of the minimum separation in the R–N plane (i.e., Fig. 8), and the first cross through the $R = 0$ axis happens at a definitely safe along-track separation (i.e., Fig. 9). Therefore, after the picosatellite orbit determination is performed on-ground through radar tracking measurements, the initial conditions of the AVANTI experiment can be achieved by slowly drifting toward the picosatellite, without the need to substantially correct both relative eccentricity and inclination vectors.

The structure of the maneuvering scheme of Eq. (17) derives from the assumptions made in the preliminary design section. Because this study addresses an open-loop scheme, a minimum number of precomputed pulses is planned, and a consistent radial maneuver has to be performed at the expense of the thruster system of BIROS. Alternative baselines can be searched by allowing the separation to involve more maneuvers. In this case, in fact, the constraints affecting the final conditions would become active only after the execution of the last maneuver. This topic has to be investigated in the attempt to reduce the size of each single maneuver and, possibly, the overall delta-v consumption.

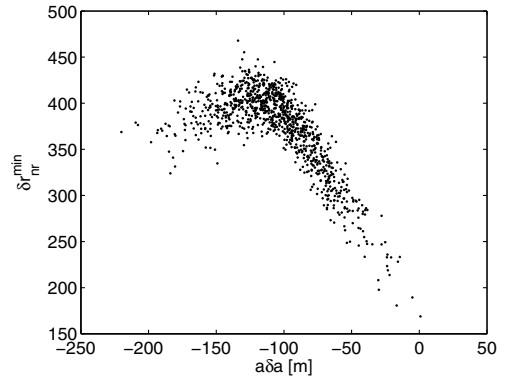

Fig. 8 Minimum cross-track distance as a function of the final $a\delta a$.

V. Conclusions

This paper addresses the design and the consequent feasibility analysis of the in-orbit release of a picosatellite from a small satellite carrier in low Earth orbit. This research embodies the prerequisite to the execution of the Autonomous Vision Approach Navigation and Target Identification experiment, scheduled for 2016. To this aim, a comprehensive overview of the mission requirements and of the operational aspects relevant to the mission safety are provided.

The peculiar scenario of aiming at a midrange stable formation while employing a release mechanism that provides a large and strongly uncertain separation delta-v demands the adaption of a well-known passive safety concept, based on the relative eccentricity/inclination vector separation, to cope with operational constraints and feasibility criteria. Specifically, the first one concerns the achievement of the minimum along-track separation to exploit a radar tracking campaign to perform relative orbit determination. Within this scenario, in fact, this represents the only available source of navigation information. The second criterion, closely related to the first one, asks the unavoidable residual drift to increase the relative separation, regardless of the magnitude and of the nature of the system's uncertainties. Finally, the last feasibility criterion is to reduce at minimum the probability of a formation evaporation, thus posing a condition in contrast with the first two.

This paper proposes a formalization of all these aforementioned safety requirements that allows addressing them already at the design level. This is accomplished by exploiting the powerful framework of the relative orbital elements. Moreover, this study supports the theoretical investigation through a numerical analysis that includes several sources of uncertainty, representative of the behavior of the space segment. As a result, a realistic assessment has been obtained that minimizes both collision and evaporation risks.

This research focuses on a double-impulse guidance strategy, where the first maneuver is provided by the deployment mechanism, and the second one is accomplished by the thrusters' system of the carrier satellite. Nevertheless, before the ultimate selection of the final mission plan, an analysis of the realistic performance of a multi-impulse separation scheme will be accomplished as well. According to the carrier thrusters' system, the involvement of a larger number of maneuvers allows distributing the needed delta-v over more but smaller burns. At a planning level, a larger range of relative configurations can be exploited in the intermediate phases because only the final relative orbit is subjected to the complete set of constraints. The introduction of additional maneuvers can lead to a larger delta-v consumption. An increased number of maneuvers allows establishing the final relative orbit by firing the thrusters only

in the tangential direction. This last point is beneficial to an overall reduction of the delta-v consumption.

References

[1] Reile, H., Lorenz, E., and Terzibaschian, T., "The FireBird Mission—A Scientific Mission for Earth Observation and Hot Spot Detection," *Small Satellites for Earth Observation, Digest of the 9th International Symposium of the International Academy of Astronautics*, Wissenschaft und Technik Verlag, Berlin, 2013, pp. 17–20.

[2] Engberg, B., Ota, J., and Suchman, J., "The OPAL Satellite Project: Continuing the Next Generation Small Satellite Development," *Proceedings of the 9th Annual AIAA/USU Conference on Small Satellites*, Paper SSC-95-V-5, Logan, UT, 1995.

[3] Puig-Suari, J., Turner, C., and Ahlgren, W., "Development of the Standard CubeSat Deployer and a CubeSat Class PicoSatellite," *Proceedings of the 2001 IEEE Aerospace Conference*, Vol. 1, IEEE Publ., Piscataway, NJ, 2001, pp. 347–353. doi:10.1109/AERO.2001.931726

[4] Ballard, P. G., Meza, A., Ritterhouse, S., Schaffer, T., Conley, C., Taylor, C., Atkine, D. D. D., and McLeroy, J. C., "Small Satellite Deployments from STS116—Development of New Manned Spaceflight Deployment Systems," *Proceedings of the AIAA/USU Conference on Small Satellites, Technical Session 3: Launch & Propulsion Systems*, Paper SSC-07-III-1, 2007.

[5] Springmann, J. C., Bertino-Reibstein, A., and Cutler, J. W., "Investigation of the On-Orbit Conjunction Between the MCubed and HRBE CubeSats," *Proceedings of the 2013 IEEE Aerospace Conference*, IEEE Publ., Piscataway, NJ, 2013, pp. 1–8. doi:10.1109/AERO.2013.6497127

[6] "Poly Picosatellite Orbital Deployer Mk III ICD," CubeSat Program, TR, 2007, http://www.oh1sa.net/data/satellite/cubesat/P-POD-mk3/P-POD%20Mk%20III%20ICD.pdf.

[7] Bodin, P., Noteborn, R., Larsson, R., Karlsson, T., D'Amico, S., Ardaens, J. S., Delpech, M., and Berges, J. C., "Prisma Formation Flying Demonstrator: Overview and Conclusions from the Nominal Mission," *35th Annual AAS Guidance and Control Conference*, American Astronautical Soc. Paper 12-072, Springfield, VA, 2012.

[8] Persson, S., D'Amico, S., and Harr, J., "Flight Results from PRISMA Formation Flying and Rendezvous Demonstration Mission," *Proceedings of the 61st International Astronautical Congress*, Curran Associates, Inc., Red Hook, NY, 2010, pp. 446–457.

[9] D'Amico, S., Montenbruck, O., Larsson, R., and Chasset, C., "GPS-Based Relative Navigation During the Separation Sequence of the PRISMA Mission," *AIAA Guidance, Navigation and Control Conference*, AIAA Paper 2008-6661, Aug. 2008.

[10] D'Amico, S., "Autonomous Formation Flying in Low Earth Orbit," Ph.D. Thesis, Technical Univ. of Delft, Delft, The Netherlands, March 2010.

[11] Härting, A., Rajasingh, C. K., Eckstein, M. C., Leibold, A. F., and Srinivasamurthy, K. N., "On the Collision Hazard of Colocated Geostationary Satellites," *AIAA/AAS Astrodynamics Conference*, AIAA Paper 1988-4239, 1988.

[12] Montenbruck, O., Kirschner, M., D'Amico, S., and Bettadpur, S., "E/I-Vector Separation for Safe Switching of the GRACE Formation," *Aerospace Science and Technology*, Vol. 10, No. 7, 2006, pp. 628–635. doi:10.1016/j.ast.2006.04.001

[13] D'Amico, S., and Montenbruck, O., "Proximity Operations of Formation Flying Spacecraft Using an Eccentricity/Inclination Vector Separation," *Journal of Guidance, Control, and Dynamics*, Vol. 29, No. 3, 2006, pp. 554–563. doi:10.2514/1.15114

[14] Spurmann, J., and D'Amico, S., "Proximity Operations of On-Orbit Servicing Spacecraft Using an Eccentricity/Inclination Vector Separation," *Proceedings of the 22nd International Symposium on Spaceflight Dynamics*, INPE Paper 034, Sao Jose dos Campos, Brazil, 2011.

[15] Gaias, G., and D'Amico, S., "Impulsive Maneuvers for Formation Reconfiguration Using Relative Orbital Elements," *Journal of Guidance, Control, and Dynamics*, Vol. 38, No. 6, 2015, pp. 1036–1049. doi:10.2514/1.G000189

[16] Gaias, G., Ardaens, J.-S., and D'Amico, S., "The Autonomous Vision Approach Navigation and Target Identification (AVANTI) Experiment: Objectives and Design," *Proceedings of the 9th International ESA Conference on Guidance, Navigation & Control Systems*, Porto, Portugal, 2014.

[17] Ardaens, J.-S., and Gaias, G., "Spaceborne Autonomous Vision-Based Navigation System for AVANTI," *Proceedings of the 65th International Astronautical Congress*, IAC Paper IAC-14.B4.7B.3, Toronto, 2014.

[18] Karlsson, T., Ahlgren, N., Faller, R., and Schlepp, B., "PRISMA Mission Control: Transferring Satellite Control Between Organisations," *Proceedings of SpaceOps 2012*, Curran Associates, Inc., Red Hook, NY, 2012, pp. 1968–1978.

[19] Kahle, R., Weigel, M., Kirschner, M., Spiridonova, S., Kahr, E., and Letsch, K., "Relative Navigation to Non-Cooperative Targets in LEO: Achievable Accuracy from Radar Tracking Measurements," *International Journal of Space Science and Engineering*, Vol. 2, No. 1, 2014, pp. 81–95. doi:10.1504/IJSPACESE.2014.060112

[20] D'Amico, S., Ardaens, J.-S., Gaias, G., Benninghoff, H., Schlepp, B., and Jø rgensen, J. L., "Noncooperative Rendezvous Using Angles-Only Optical Navigation: System Design and Flight Results," *Journal of Guidance, Control, and Dynamics*, Vol. 36, No. 6, 2013, pp. 1576–1595. doi:10.2514/1.59236

[21] Clohessy, W. H., and Wiltshire, R. S., "Terminal Guidance System for Satellite Rendezvous," *Journal of the Aerospace Sciences*, Vol. 27, No. 9, 1960, pp. 653–658. doi:10.2514/8.8704

[22] D'Amico, S., "Relative Orbital Elements as Integration Constants of Hill's Equations," DLR, German Aerospace Center TN-05-08, Oberpfaffenhofen, Germany, Dec. 2005.

E. G. Lightsey
Associate Editor